



Synthesis and Characterization of Novel CaO-based Heterogeneous Catalysts for Efficient Biodiesel Production from Waste Cooking Oil

Rasha Alaa Eldine^a, Hosam H. Abdelhady^{a,*}, Sahar Abd Elhafez^b,

Mohamed S. El-Deab^{a,*}



CrossMark

^a Chemistry Department, Faculty of Science, Cairo University, Cairo, Egypt.

^b Ghamra Research Center, Egyptian Petroleum Authority, Cairo, Egypt.

Abstract

In this study, a series of novel basic heterogeneous catalysts (Ca-based mixed Ce and Cu oxides) with various mass ratios were designed by co-precipitation method to be utilized in biodiesel, Fatty acid methyl ester (FAME) production via the transesterification process of waste oil under the following process conditions (i.e., methanol to waste cooking oil mass ratio of [13:1] at reaction temperature 75 °C for 5 h). The various binary mixed oxides were characterized by several techniques (e.g., Thermo-gravimetric analysis (TGA-DTG), powder X-ray diffraction (XRD), Brunauer-Emmett-Teller (BET) surface area measurements, Fourier transform- Infrared (FT-IR) spectroscopy, and surface basicity by back titration). Biodiesel yield is estimated by gas chromatography (GC). The biodiesel optimum yield, of 95 and 94 % yield is achieved by 3CaO-1CeO₂@800 °C and 3CaO-1CuO@800 °C catalysts under the reaction condition of 2% wt. catalyst loading level, methanol to waste oil molar ratio of [13:1], reaction temperature of 75 °C, and reaction time of 2 h for the former catalyst, while, catalyst loading of 2% for 1 h at 75 °C and [13:1] M:O molar ratio for the later one, respectively. The high catalytic activity may be attributed to the higher BET surface area and strong basic characteristics, which indicate more accessible active sites for the transesterification process on the catalyst surface. Furthermore, the catalytic materials were reactivated and reused for two to three reaction cycles. The physical characteristics of the produced FAME are found to fulfill the American standard for testing materials (ASTM D-6751) international standards.:

Keywords: Transesterification; Biofuel; CaO; CeO₂; CuO; FAME; Basicity.

1. Introduction

Every area of a country's economic development is dependent on energy. As a result, energy demand has steadily risen along with industrialization and human population growth. Petroleum, coal, and natural gas are the three most vastly utilized combustible resources. Energy security is a big concern for every government due to the rising cost of combustible materials and the future shortage prospects [1,2]. Furthermore, utilizing fossil fuels has several drawbacks, including air pollution and environmental problems. In the same vein, emissions from combustibles are a significant source of greenhouse gases and air pollutants (including CO,

NO_x, SO_x, hydrocarbons, particulates, and chemicals that cause cancer), which is considered the key reason for the global warming crisis. The drawbacks and scarcity of fossil fuels have urged a lot of stakeholders to alternative renewable energy resources [1–4]. Indeed, the usage of biomass-based renewable and sustainable energy resources made from waste feedstock has increased owing to the depletion of petroleum reserves. Consequently, the use of biodiesel has been noted as one of the most forceful prospective biofuel sources. The merit retained from using biodiesel products is thus a fuel with properties similar to Petro-diesel, which enables it to be utilized in existing Petro-diesel machines

*Corresponding author e-mail: hosamhasan88@cu.edu.eg (H. Abdelhady), msaada@cu.edu.eg (M. S. El-Deab).

Received date 01 November 2023; revised date 24 December 2023; accepted date 30 January 2024

DOI: 10.21608/EJCHEM.2024.246023.8807

©2024 National Information and Documentation Center (NIDOC)

even without engine modifications to get rid of its complexities [5–8].

Currently, most biodiesel generated globally is produced from the transesterification of animal fats (AFs), vegetable oils (VOs), and recycled greases (RGs) via the reaction with methanol (or small alcohol molecules) in the presence of a catalyst, giving up glycerol, a valuable by-product that can be utilized in many cosmetics beside it can be also employed electro-oxidation in glycerol fuel cells [9–13], beside the main component biodiesel. According to the pretreatment procedures, these resources comprise triglycerides (TGs), free fatty acids (FFAs), and other impurities [14].

Transesterification is typically a catalyzed chemical reaction by base-, acid-catalyzed transesterification or enzymes. Since there are many different feedstock systems, this study focuses on reviewing the impact of the main reaction conditions to produce biodiesel as well as summarizing the advantages and disadvantages of these key transesterification processes [15–21].

Indeed, there are two essential types of catalysts in FAME production which are homogeneous acid/base catalysis such as NaOH, and KOH, and heterogeneous acid/base catalysis (e.g., metal oxides, hetero-poly-acids ... etc.). The advantages of using a base homogeneous catalyst (NaOH, KOH ...etc.) are that the reaction proceeds much faster, shows a high yield, and has lower corrosion toxicity than the homogeneous acid (e.g., H₂SO₄) catalyst. After the process completion, the reaction mixture must be neutralized and washed with an enormous amount of water to get rid of the resultant salt [22,23]. On the contrary, the majority of biodiesel is produced commercially utilizing homogenous base catalysts which have some demerits (e.g., wasteful, corrosive, and non-recyclable, increasing the overall expenses, and have an environmental impact, ...etc.) that must be counteracted, [24–26].

A heterogeneous catalyst is a respectable substitute for homo-catalysts in the transesterification of VOs for the FAME production owing to the verity that a solid hetero-catalyst wouldn't fuse in the reaction mixture, so it is easy to remove and separate from the yield and reused but the elimination of homo-catalysts is a problematic beside that huge amount of wastewater is resulting through the process and desires to be handled by neutralization procedure

so that the homo-catalysts are predictable to be substituted with solid hetero-catalyst owing to environmental and economics causes in the adjacent future.

Industrialization of biodiesel has been strongly encouraged in the last decade but the biggest impediment is the economics of its production. This is mostly owing to the expensive feedstocks because of the higher charge of virgin VOs [27,28] Obviously, about 60 — 80% of the charge of producing FAME is related to chemical prices. Due to competition between the market for human consumption and biodiesel, VOs may turn into more costly. Scholars have concentrated on using non-edible triglycerides to produce FAME to get around these limitations [29].

The use of WCO as a FAME resource has no battle with feed practice. Waste-frying oils (WFOs) could be classified into yellow and brown greases. Yellow grease, with free fatty acid (FFAs) contents \leq 15%, resulting from WFOs, AFs, and WCO gathered from local restaurants or commercial cooking processes, offers considerable possible low-cost feedstock for FAME production [30]. Alkaline-catalyzed transesterification [31–34] acid-catalyzed transesterification [35–38], two-step transesterification [39,40] enzymatic catalysis [41–43] and supercritical alcohol processing [14,29] are all practices for processing WCO into FAME [44–48].

The present work inspected the behaviors of sundry binary metal oxides of Ca-based solid hetero-catalysts (Ca with CuO or CeO₂ oxides) in the methanolysis of WCO for FAME production and the effect of the basicity of these binary oxides on the FAME yield. All predecessors were prepared by using the co-precipitation technique, where after thermal treatment, the corresponding binary Ca-based metal oxides were attained. Various techniques were utilized for the determination of textural, structural, and basal features of the proposed catalysts.

2. Materials and Methods:

2.1. Materials:

The chemicals utilized in the current study were obtained from European Union EU and Indian Companies, CaCl₂, (BDH, 99.5%), ceric ammonium nitrate (NH₄)₂[Ce(NO₃)₆] (Indian Company- 98%), copper nitrate Cu(NO₃)₂.3H₂O, (were used as a precursor of metal oxide), while NaOH (Indian

Company- 98%) were used for catalyst pretreatment, and methanol (99.9%) was purchased from EU Company.

WCO was provided by regional restaurants for fried food in Cairo, Egypt to be employed as a triglyceride feedstock. The WCO was filtered to get rid of residues and insoluble scums, then heated at 110 °C overnight to remove any water, centrifuged to remove the waxes then the separated upper layer of oil was collected to study the physical and chemical features of WCO following standard test methods ASTM [49,50]

2.2. Catalyst Preparation and Characterization:

2.2.1. Catalyst Preparation

The precursor calcium chloride (CaCl_2), ceric ammonium nitrate $(\text{NH}_4)_2[\text{Ce}(\text{NO}_3)_6]$, copper nitrate $\text{Cu}(\text{NO}_3)_2 \cdot 3\text{H}_2\text{O}$, were used as the parent compound for preparing the hydroxides $\text{M}(\text{OH})_x$ [$\text{M} = \text{Ca}, \text{Ce}, \text{Cu}$] by simple gel-formation via a co-precipitation technique using NaOH until complete precipitation occurs within 2 h. while adjusting $\text{pH} = 10\text{--}12$. The resulting precipitate was agitated for 1 h at ambient temperature, aged overnight, washed, and filtered at least 6 times, and dried out in a drying kiln at 100 °C for 6 hours to attain $\text{M}(\text{OH})_x$. The dried precipitate was thermally treated in air at 500 or 800 °C for 4 h, respectively. The catalyst after thermal treatment was milled to get uniform-sized particles.

In this work, a series of novel binary mixed metal oxide catalysts are synthesized by a modest gel-formation via a co-precipitation technique to boost the interplay of catalyst components with the surface features of the catalyst as follows: 1.0 M of the binary metal nitrate solutions were homogeneously blended in various mass proportions of catalysts is nominated as $[x\text{M}^1\text{O} - y\text{M}^2\text{O}]$, while M^1 and M^2 are assigned to 1st and 2nd metal, respectively]. By calculation of the desired amount of two metal nitrate salts were dissolved in a determined amount of distilled H_2O and then agitated together for 2 h, after that the aqueous solution of sodium hydroxide, NaOH (2M) was added in a dropwise fashion to the above solution of mixed nitrates with vigorous stirring until complete precipitation occurs within 2 h while adjusting $\text{pH} = 10\text{--}12$. The resulting solution was agitated for 1 h after complete

precipitation, then aged for 24 h, filtered, washed at least 6 times, and then dried out in a drying kiln at 100 °C for 2h. The dried precipitate was then calcified in air at 500/800 °C for 4 h. The catalyst after calcination was grained to get uniform-sized particles.

2.2.2- Catalyst characterization

(I) Thermo-gravimetric analysis (TGA)/Differential Thermo-gravimetric Analysis (DTG)

Thermo-gravimetric analysis (TGA)/Differential Thermo-gravimetric Analysis (DTG) was employed for monitoring the thermic stability of the as-prepared substance in which the mass of the catalyst was observed as a cursor of temperature, Thermal decomposition was inspected by a Shimadzu 50H TG/DTG thermal-analyzer in a dynamic atmosphere of airflow. Measurement surroundings were typical sample mass of 10 ± 0.5 mg, with a ramping rate of 10 °C min^{-1} and changing the temperature as of 40 - 1000 °C.

(II) Fourier Transform Infrared (FT-IR)

Fourier Transform Infrared (FT-IR) spectroscopy (ALPHA, Bruker, Germany) was utilized to afford information about the functional group of the as-prepared catalytic material. The specimen was inspected in the range of 400 – 4000 cm^{-1} . The infrared scanning was done at 298 K with a 2 cm^{-1} resolution.

(III) X-ray diffraction (XRD)

The XRD has been utilized in two main areas, for the characterization of crystalline materials and the determination of the crystallite size. Each crystalline solid has its distinct characteristic X-ray powder pattern which may be employed as a "fingerprint" to identify it. The crystal framework of the as-prepared nano-catalysts was recorded (an accelerating voltage of 40 kV, and a current of 30 mA). X-ray diffractometer, using a Cu (K_α) radiation source ($\lambda = 1.5418 \text{ \AA}$) which joined with the Ni filter in the 2θ of 5-80° range. Powder diffraction data is maintained in files known as ICSD -Cards. The data in these files are in terms of (d) spacing and relative line intensities.

The crystallite size was attained by utilizing Debye's Scherrer equation (eq. 1):

$$D_p = \frac{K \lambda}{\beta \cos(\theta)} \quad (1)$$

where D_p , the crystal size, λ is the X-ray wavelength (Cu-K α = 1.5418 Å), K is the shape factor (≈ 0.9), β is line broadening intensity (the full width at half the maximum (FWHM)) in radians and θ is the Bragg diffraction angle.

(IV) BET surface area measurements

The surface area measurements of the as-prepared catalysts were examined by Brunauer-Emmet-Teller (BET) by a multiple BET method, which relies on the estimation of the quantity of physically adsorbed N_2 on the catalyst's exterior at the temperature of liquid N_2 (-196°C). The total pore volume and specific surface area were estimated using an N_2 -adsorption-desorption isotherm at liquid N_2 (temperature = -196°C), using a NOVA 2200 instrument (Quantachrome, USA). Former to the adsorption-desorption measurements, all the specimens were degassed at 300°C overnight to get rid of further adsorbates and moisture. The surface area of a sample is specified by the physical adsorption of a gas on the exterior of the solid and by calculating the quantity of adsorbate gas matching to a mono (molecular) layer on the exterior surface, the data is determined according to BET adsorption isotherm equation (see Eq. 2):

$$\frac{P}{V(P_o - P)} = \frac{1}{V_m C} + \left[\frac{(C - 1)}{V_m C} \right] \frac{P}{P_o} \quad (2)$$

where: P = the adsorbate gas partial vapor pressure which is in equilibrium with the exterior at 77.4 K (Boiling point of liquid N_2), in Pascal, V = the adsorbed gas volume at STP [273.15 K and atm. pressure (1.013×10^5 Pa)], in milliliters, P_o = adsorbate gas saturated pressure, in Pascal, V_m = adsorbed gas apparent monolayer volume at STP, in milliliters, C = dimensionless constant that is connected to the adsorption enthalpy of the adsorbate gas on the specimen.

(V) Scanning electron microscopy (SEM)

The morphology of the several catalytic materials was revealed using field emission-scanning electron microscopy (FE-SEM-QUANTA FEG 250) connected with EDX Unit (Energy Dispersive X-ray Analyses).

(VI) Basicity Measurements

Surface basicity was estimated by the back-titration method, this method was utilized to probe the basicity/acidity of the as-synthesized catalytic materials. For determination of basic characteristics, the catalytic material was blended with an excess identified concentration of hydrochloric acid where the basic catalytic material neutralizes the hydrochloric acid by an equal volume to its basic characteristic, then the excess hydrochloric acid was titrated against the known concentration of NaOH. Lastly, the amount of hydrochloric acid balanced by the sample is estimated and expressed as the total basicity of the catalyst as mmol of hydrochloric acid /g of catalyst (Eq. 3),

$$\text{Basicity} \left[\frac{\text{mmol}}{\text{g}} \right] = \frac{(N \times V)_{\text{titrant}}}{[\text{wt of catalyst (g)}]} \times 1000 \quad (3)$$

where N : is the normality of sodium hydroxide (1 g equ. L^{-1}) and V : is the volume of sodium hydroxide (L).

2.3. Catalytic activity test

2.3.1. Biodiesel production by using the transesterification method.

Transesterification of the WCO process relies on several factors such as type and quantity of the utilized alcohol, reaction time and temperature, rate of agitation and catalyst concentration, and FFA percentage in the feed WCO. The optimal values of these factors to attain the maximum conversion depend on the physico-chemical features of the feedstock WCO.

The methanolysis reaction was conducted utilizing the following environments: 10 g of the WCO was charged in a 25 mL round flask, where various molar proportions of methanol to WCO, as well as various weight percent (concerning the WCO) of the solid catalysts, were fed into the reaction pot as a batch vessel with a thermocouple junction on hotplate stirrer. The reaction was started by charging various weight percent of the as-synthesized catalyst, and the reaction was run for 1-5 h. The reactants were stirred at a fixed agitation speed of 300 revolutions per minute while the reaction temperature was maintained at $75 \pm 2^\circ\text{C}$ for the desired reaction time. After the process completion, the reaction blend was centrifuged after cooling to remove the solid hetero-catalyst from the FAME-glycerol mixture. Then the methanol was removed from the blend in a drying kiln at 70°C . The reaction samples were sampled at fixed time intervals (1, 2, 3, 4, and 5 h) and the yield of the FAME was calculated utilizing the gas chromatography (GC) practice (C.f. Eq. 4).

2.3.2. Biodiesel yield evaluation process

The produced FAME was identified and characterized utilizing GC-Agilent 7890A, FID flame ionization detector equipped with Agilent HP-5 column (5% phenyl methyl silox) [column dimensions of 30 m x 250 μ m x 0.25 μ m] and helium as a gas transporter. Additionally, to confirm the identified FAME by GC, 10 μ L were taken of the internal standard dissolved in toluene (1ml) to make the standard solution. 100 μ L of the ready sample was mixed with the standard solution, and then 0.1 μ L specimen was inserted into the GC. The parameters of the kiln temperature program [60 $^{\circ}$ C with 2 min (hold time)-2 min (runtime)], [10 $^{\circ}$ C/min temperature ramp rate up to 180 $^{\circ}$ C - 0 minute (hold time) -14 min (runtime)], [5 $^{\circ}$ C/min up to 250 $^{\circ}$ C with 7 minutes (hold time)]. The FAME yield is obviously the same as that of the FAME % estimated quantitatively by GC. The FAME yield (%) was calculated according to the Eq. 4:

$$FAME\ yield = \frac{(\Sigma A) - A_{IS}}{A_{IS}} \times \frac{C_{IS} \times V_{IS}}{W} \times 100\% \quad (4)$$

where ΣA = the total peak area of methyl ester, A_{IS} = peak area of the internal standard, C_{IS} = concentration (mg. ml⁻¹) of the internal standard solution, V_{IS} = volume (ml) of the internal standard solution, W = weight of sample in mg.

2.3.3 Reusability test analysis

A catalyst reusability test is very important to show the advantage of using a catalyst to reduce the production cost for its use in industrial applications. The reusability of the as-prepared calcined catalyst was studied with the conditions of the sample with the highest yield. After each cycle the catalyst was decanted from the reaction mixture by centrifugation, washed with n-hexane more than a time, and dried overnight in an oven at 100 $^{\circ}$ C.

3. Results and discussion:

3.1. Characterization of the proposed catalyst:

3.1.1 Thermo-gravimetric Analysis (TGA):

The thermal decomposition of the various binary metal hydroxides utilized in this study is displayed in Fig. 1 (a-f).

Fig. 1 (a-c) displays the TGA curve and its derivative of a series of binary metal hydroxide precursor $x\text{Ca}(\text{OH})_2\text{-}y\text{Ce}(\text{OH})_4$ with different mass

ratios to study the thermal decomposition of these catalyst precursors. The binary metal hydroxide $1\text{Ca}(\text{OH})_2\text{-}3\text{Ce}(\text{OH})_4$ show a two-stage decomposition fashion. The first decomposition was observed in the range [100 – 120 $^{\circ}$ C] with weight loss (\approx 10%) from the TGA % curve accompanied by an endothermic peak due to dehydration of moisture and impurities (physical desorption). The 2nd decomposition phase with a weight loss of (\approx 18%) from the TGA curve in the temperature range of (750 – 800 $^{\circ}$ C) may be ascribed to the decomposition of binary hydroxide due to chemical decomposition and releasing water molecules. While The TGA and Dr-TGA curves of the binary mixed hydroxide $2\text{Ca}(\text{OH})_2\text{-}2\text{Ce}(\text{OH})_4$ & $3\text{Ca}(\text{OH})_2\text{-}1\text{Ce}(\text{OH})_4$ show complete breakdown through one stage characteristic to weight loss at 14% and 32%, respectively, accompanied by endothermic peaks at 670 and 800.

Fig. 2 (d-f) shows the TGA and Dr-TGA curves of the second binary hydroxide $x\text{Ca}\text{-}y\text{Cu}(\text{OH})_2$ with different mass ratios, in this event the binary hydroxide $1\text{Ca}(\text{OH})_2\text{-}3\text{Cu}(\text{OH})_2$, showing complete decomposition through two stages. The first decomposition step was located at \approx 200 $^{\circ}$ C which may be attributed to loss of moisture, and physical desorption, the second and third ones indicated the start of hydroxide decomposition between (750 $^{\circ}$ C), characteristic of weight loss at 55%, the binary hydroxide $2\text{Ca}(\text{OH})_2\text{-}2\text{Cu}(\text{OH})_2$, decomposes through three-step, the first one in the range (100-200 $^{\circ}$ C), the second and the third one may be ascribed to complete decomposition cause of chemical desorption and form the binary oxide at [600-850 $^{\circ}$ C] characteristic to weight loss at 20% and the binary hydroxide $3\text{Ca}(\text{OH})_2\text{-}1\text{Cu}(\text{OH})_2$ shown disintegration through three steps, the first one due to loss of moisture and impurities but the second and the third one indicate complete decomposition into mixed oxide (800-1000 $^{\circ}$ C) characteristic to weight loss at 95%.

3.1.2. FT-IR Spectra

The FT-IR spectra are displayed in Fig. 2, respectively. Fig. 2(a-b) represents the binary mixed oxide $x\text{CaO}\text{-}y\text{CeO}_2$ calcined at 500 / 800 $^{\circ}$ C for 4h, with different mass ratios, respectively. The bands that appeared at 3650 and 3880 cm^{-1} may be ascribed to asymmetric and symmetric stretching modes of the adsorbed water molecules on the exterior of binary metal oxide. The broadband revealed at 1400 -1500 cm^{-1} indicated the C-O bond correlated to the

carbonization of the CaO nanoparticles. Symmetric stretching bands between $880 - 890 \text{ cm}^{-1}$ and $708 - 715 \text{ cm}^{-1}$ may be addressed to surface CO_3^{2-} contaminants. The broadband appears around $400 - 450 \text{ cm}^{-1}$, corresponding to the Ca-O bond with the appearance of a new Ce-O-Ce stretching vibration band.

FT-IR spectra analysis displayed in Fig. 2 (c-d) represents the binary $x\text{CaO}-y\text{CuO}$ binary oxide at calcination temperature $500/800 \text{ }^\circ\text{C}$ for 4 h, with different mass ratios, respectively. Noticed that the bands appeared at $3655, 1425-1450, 880 - 890, 665-720$, and $400 - 525 \text{ cm}^{-1}$, The spectra show an absorption girdle at $665-720 \text{ cm}^{-1}$ which is attributed to vibration of Cu-(II)-O confirming the formation of nanoparticles, while the peak appears at $400-525 \text{ cm}^{-1}$ can be allocated to the CaO stretch vibration[51].

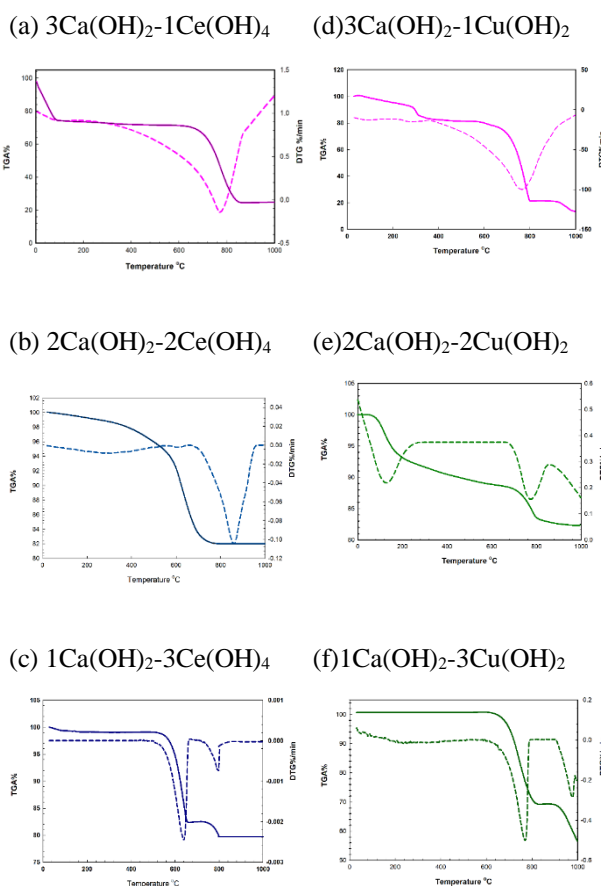


Fig. 1: (a-f) TGA and Dr-TGA of the as-prepared binary hydroxide (a-c) binary $x\text{Ca}(\text{OH})_2 - y \text{Ce}(\text{OH})_4$ and (d-f) binary $x\text{Ca}(\text{OH})_2 - y \text{Cu}(\text{OH})_2$.

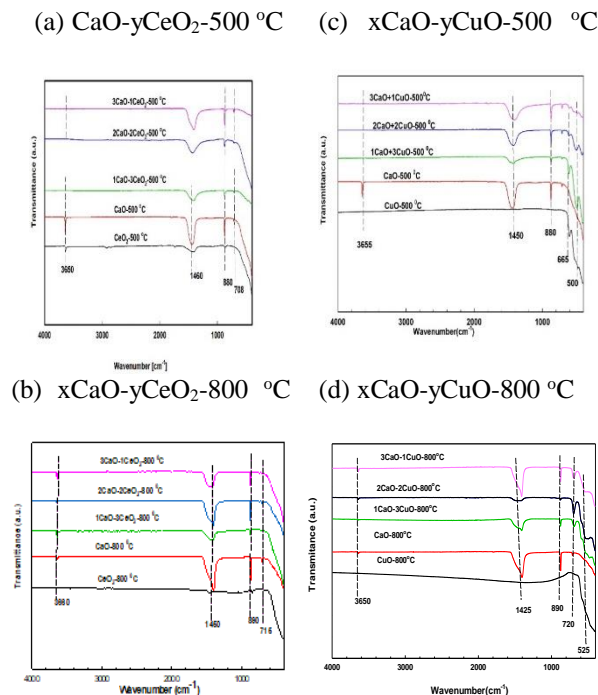


Fig. 2: FT-IR spectra of (a) binary $x\text{CaO}-y\text{CeO}_2$ calcined at $500 \text{ }^\circ\text{C}$, (b) binary $x\text{CaO}-y\text{CeO}_2$ calcined at $800 \text{ }^\circ\text{C}$, (c) binary $x\text{CaO}-y\text{CuO}$ calcined at $500 \text{ }^\circ\text{C}$, and (d) binary $x\text{CaO}-y\text{CuO}$ calcined at $800 \text{ }^\circ\text{C}$.

3.1.3. X-ray diffraction (XRD)

Fig. 3 (a-b) displays the XRD diffraction patterns of binary $x\text{CaO}-y\text{CeO}_2$ oxides, Fig. 3 (c-d) displays the XRD diffraction patterns of binary $x\text{CaO}-y\text{CuO}$ binary oxides, calcined at $500 / 800 \text{ }^\circ\text{C}$ for 4 h. The neat CaO provided narrow and well-defined diffraction crystalline peaks at $2\theta = 32.25^\circ, 34.17^\circ, 37.44^\circ, 53.91^\circ, 64.21^\circ, 67.45^\circ$ structure complementary with miller indices (hkl) of (111), (101), (200), (220), (311) and (222) planes this comply with the other value ICSD of CaO card no. = [00-043-1001], but $\text{Ca}(\text{OH})_2$ reveals diffraction peaks centered at $2\theta = 18.06^\circ, 29.48^\circ$, accompanied by miller indices (hkl) (001), (100), respectively, which may be due to moisture abstraction by CaO this in agreement with ICSD card no.=[00-044-1481], [52].

XRD Diffraction peaks of pure CeO_2 were observed at $2\theta = 28.5, 33.1, 47.48, 56.32, 59.1, 69.6,$ and 76.9° along with (hkl) indices of (111), (200), (220), (311), (222), (400), and (311) planes, consequently. which confirmed the formation of CeO_2 nanoparticles with face-centered cubic crystal

structure and the attained results agreed with ICSD card no. [01-080-4829] [53].

In the XRD profiles of the mixed binary oxide at 500/ 800°C) $x\text{CaO}-y\text{CeO}_2$ (show individual phases of CeO_2 and CaO were observed without producing new compounds. The rise in CaO content caused a growth and a slight reduction in the peak intensities of CaO and CeO_2 , respectively. This may be assigned to the coating of the ceria surface with Ca^{2+} species that results in a developed X-ray scattering factor of Ca^{2+} in comparison with the Ce^{4+} ions [53,54]. Originally, the mixing of the Ca component with the CeO_2 crystalline structure at a low loading level might be firstly set between the CeO_2 granules borders and thus bothered the usual growth of the CeO_2 crystallites at high loading levels and high temperature (c.f. Table 1),

The XRD diffraction patterns of the $\text{CaO}-\text{CuO}$ binary catalytic materials with distinct mass ratios of CaO and CuO at different calcination temperatures are shown in Fig. 3) c-d), respectively. The XRD patterns clearly show the existence of a blend of CaO , and CuO and contaminated with traces of $\text{Ca}(\text{OH})_2$. The X-ray diffraction patterns confirmed the establishment of CuO nanoparticles with monoclinic crystal structure and the attained results are compatible with the ICSD card number [04-004-5425]. Diffraction peaks were observed along (110), (002), (200), (-202), (020), (202), (-113), (-311), and (220) planes. The monoclinic crystal type structure of pure CuO showed the characteristic reflection at the d-space value at $2\theta = 32.62^\circ, 35.70^\circ, 38.86^\circ, 48.88^\circ, 53.56^\circ, 58.44^\circ, 61.60^\circ, 66.38^\circ, \text{ and } 68.23^\circ$. It is clearly observed that the CuO mean crystal size decreased steadily with the calcium loading from lower to higher concentrations leading to higher surface area as will be discussed below in the next session (C.F. Table 1) [54].

3.1.4. BET-Surface area measurements and pore size distribution.

The pore size, pore volume, and specific surface area measurements were estimated by using the BET - method of $x\text{CaO}-y\text{CeO}_2$ and $x\text{CaO}-y\text{CuO}$ samples thermally treated at 500 / 800 °C, respectively, are listed in Tables 2 and 3.

In the case of the binary oxides $x\text{CaO}-y\text{CeO}_2$, the surface area increases as the calcination temperature and CaO ratio increase, the pore volume increases as the temperature of calcination increases, while the

average particle radius decreases with the increment in Ca mass ratio.

BET-specific surface area measurement of the $3\text{CaO}-1\text{CeO}_2$ binary oxides catalysts was about $15-19 \text{ m}^2 \text{ g}^{-1}$. While BET-specific surface area measurement of the $x\text{CaO}-y\text{CeO}_2$ binary oxides catalysts is compatible with their corresponding crystallite dimensions while smaller crystallite dimensions result in higher specific surface area [55]. In the case of mixed binary oxides $3\text{CaO}-1\text{CuO}$ calcined at 500/800 °C, adsorption and desorption isotherms of the mixed oxide are of type IV [56]. The BET-specific surface area of the as-prepared catalytic materials increases from 19 at 500 °C to 20 at 800 °C. As well as the BET-specific surface area rises with the increment of the CaO ratio in the catalytic material from 1 to 3. The pore volume decreases as the temperature increases from 500 to 800 °C.

3.1.5. SEM- Mapping EDX analysis

SEM images of the mixed oxide $3\text{CaO}-1\text{CeO}_2$ are displayed in Fig 4. (a-e). SEM images of $3\text{CaO}-1\text{CeO}_2$ at different magnifications, (f-h). Mapping EDX overlay of Ca , Ce , O , respectively, (i-j) EDX of $3\text{CaO}-1\text{CeO}_2$. The SEM graph reveals that the as-synthesized catalyst has a clear morphology with uniform size. The spongy structure together with macro- and meso-pores is quite supportive of the methanolysis reaction. Those macro-pores permit triglycerides with higher molar mass to penetrate intensely into the pores of the prepared catalyst that is they could approach active basic sites on the catalyst exterior. Moreover, the mesopores improve the pore volume and specific surface area of the catalyst, which advances the total quantity of basic sites [56].

3.1.7. Catalyst activity by transesterification method:

The catalyst activity was examined by making the methanolysis reaction of WCO according to the procedure. All experiments were conducted utilizing the following conditions: calcination temperature of 500 and 800 °C, catalyst loading level 2 – 8%, and reaction time ranging from 1 – 5 h while keeping the M:O molar ratio at [13:1], reaction temperature of 75 °C, and stirring rate of 300 rpm.

The impact of $x\text{CaO}-y\text{CeO}_2$ mixed oxides calcination temperature on the FAME yield was studied at 500 and 800 °C

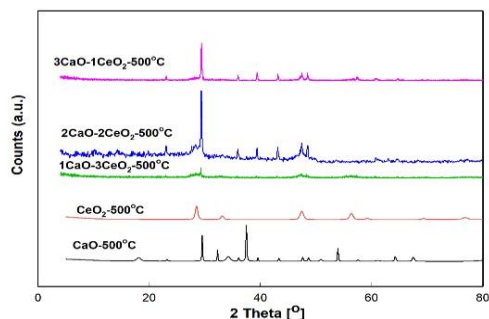
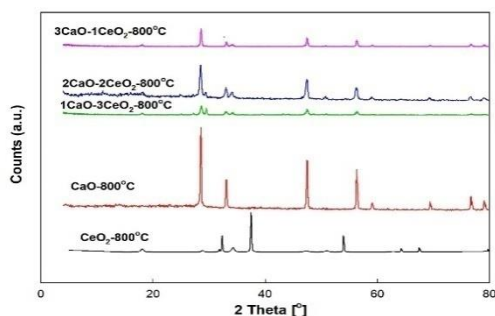
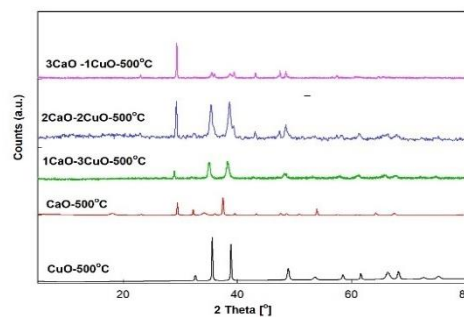
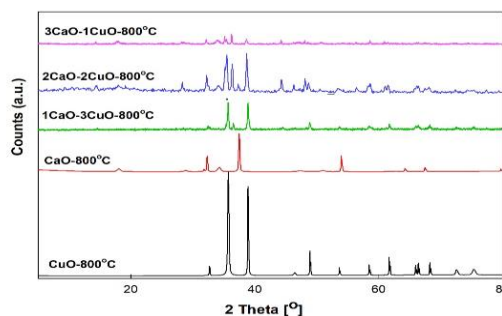
(a) $x\text{CaO}-y\text{CeO}_2-500^\circ\text{C}$ (b) $x\text{CaO}-y\text{CeO}_2-800^\circ\text{C}$ (C) $x\text{CaO}-y\text{CuO}-500^\circ\text{C}$ (d) $x\text{CaO}-y\text{CuO}-800^\circ\text{C}1.5$ 

Fig.3: XRD patterns of binary $\text{CaO}-\text{CeO}_2$, and $\text{CaO}-\text{CeO}_2$ mixed oxide (a) binary $x\text{CaO}-y\text{CeO}_2$ calcined at 500°C , (b) binary $x\text{CaO}-y\text{CeO}_2$ calcined at 800°C , (c) binary $x\text{CaO}-y\text{CuO}$ calcined at 500°C , and (d) binary $x\text{CaO}-y\text{CuO}$ calcined at 800°C .

It was noticed that upon raising the calcination temperature from 500°C to 800°C the FAME yield markedly increases from 4-11% at 500°C to 91-95% at 800°C . This tendency could be clarified by the advantageous impact of the higher temperatures on the interaction of the binary metal oxides. As well, this boosted interaction might reduce the metal oxide leakage. Therefore, the best thermal treatment temperature is 800°C .

As displayed in Tables 3 and 4, the pore volume and BET-specific surface area developed with a rise in the calcination temperature, resulting in a boosted catalytic activity for the specimens calcified at 800°C [58].

3.1.7.1 The effect of the catalyst loading level at different calcination temperatures.

The amount of catalyst used has a vital role in the biodiesel production process by the methanolysis process. In the current study the impact of the loading level of the catalyst used on the yield of FAME was

Table 1: XRD crystallite sizes of binary oxides $x\text{CaO}-y\text{CeO}_2$ and $x\text{CaO}-y\text{CuO}$ calcinated at 500°C and 800°C , respectively.

Sample	XRD-particle size, nm	Sample	XRD-particle size, nm
$\text{CaO}-500^\circ\text{C}$	44	$\text{CaO}-500^\circ\text{C}$	44
$\text{CeO}_2-500^\circ\text{C}$	55	$\text{CuO}-500^\circ\text{C}$	53
$\text{CaO}-800^\circ\text{C}$	45	$\text{CaO}-800^\circ\text{C}$	45
$\text{CeO}_2-800^\circ\text{C}$	55	$\text{CuO}-800^\circ\text{C}$	54
$1\text{CaO}-3\text{CeO}_2-500^\circ\text{C}$	44	$1\text{CaO}-3\text{CuO}-500^\circ\text{C}$	50
$2\text{CaO}-2\text{CeO}_2-500^\circ\text{C}$	43	$2\text{CaO}-2\text{CuO}-500^\circ\text{C}$	48
$3\text{CaO}-1\text{CeO}_2-500^\circ\text{C}$	43	$3\text{CaO}-1\text{CuO}-500^\circ\text{C}$	44
$1\text{CaO}-3\text{CeO}_2-800^\circ\text{C}$	49	$1\text{CaO}-3\text{CuO}-800^\circ\text{C}$	49
$2\text{CaO}-2\text{CeO}_2-800^\circ\text{C}$	48	$2\text{CaO}-2\text{CuO}-800^\circ\text{C}$	47
$3\text{CaO}-1\text{CeO}_2-800^\circ\text{C}$	39	$3\text{CaO}-1\text{CuO}-800^\circ\text{C}$	44

Table 2: BET measurements of binary oxide xCaO-yCeO₂ at 500/800 °C.

Name of sample	BET surface area-m ² /g	Average pore size (nm)
CaO-500 °C	15	12
CeO ₂ -500 °C	7	5
CaO-800 °C	18	17
CeO ₂ -800 °C	9	3
1CaO-3CeO ₂ -500 °C	13	2
2CaO-2CeO ₂ -500 °C	14	2
3CaO-1CeO ₂ -500 °C	15	3
1CaO-3CeO ₂ -800 °C	14	4
2CaO-2CeO ₂ -800 °C	14	2
3CaO-1CeO ₂ -800 °C	19	3

Table 3: BET measurements of binary oxide xCaO-yCuO at 500/800 °C.

Name of sample	BET surface area-m ² g ⁻¹	Average pore size nm
CaO-500 °C	15	12
CuO-500 °C	5	4
CaO-800 °C	18	17
CuO-800 °C	11	2
1CaO-3CuO-500 °C	14	3
2CaO-2CuO-500 °C	16	4
3CaO-1CuO-500 °C	19	3
1CaO-3CuO-800 °C	14	2
2CaO-2CuO-800 °C	18	2
3CaO-1CuO-800 °C	20	4

inspected at two different calcination temperatures (500/800 °C) by varying the catalyst loading level from 2-8 % (w/w% concerning WCO) and keeping the reaction temperature unchanged at 75 °C, reaction time at 5 h and methanol to oil mass ratio at 13:1, the yield of FAME.

It is obviously shown that the catalyst calcified at 500 °C shows a slight increase in FAME yield (<30%) even upon increasing the catalyst loading by 2–8%. Furthermore, the results of the catalyst calcined at 800 °C (see Fig. 5-6) showed that the FAME yield rises steeply as the catalyst concentration increases which may be ascribed to a growth in the number of active sites. While, when the catalyst amount exceeds a limiting amount, the FAME yield kept unchanged in the case of Ca-Ce catalysts while it decreased in the case of Ca-Cu catalysts. This influence may be assigned to the deprived diffusion between methanol, WCO, and catalyst systems [59].

3.1.7.2 Effect of reaction time at different calcination temperatures

The influence of the reaction time is another important criterion that will affect the yield of biodiesel. The less the transesterification time, the more cost-effective the process. Thus, it is observed at early reaction times (See Fig. 7-8), that alcohol molecules are distributed gently in the WCO. The FAME production yield using xCaO-yCeO₂ and xCaO-yCuO calcined at 800 °C increased from 0 % to up to ≈ 95% with the progress of reaction time from 1 – 5 h. While the ones calcined at 500 °C showed a little bit of increase in FAME yield not more than 10%. This may be due to the reaction time progress, the WCO and methanol have sufficient time to interact with each other, resulting in enhanced biodiesel efficiency [56]. After 4 h, the boosting in biodiesel yield was small owing to the reversible nature of the methanolysis reaction.

3.2. Catalyst reusability study

Catalyst reusability is one of the considerable traits of hetero-catalysts. Herein, A study on the capability of best catalyst reusability was conducted under the optimum conditions. The catalytic material attained after the end of the methanolysis process was washed with n-hexane and then dried out (overnight) in a hot air kiln (105 °C). However, the FAME conversion was drastically dropped after the 1st cycle which may be owing to the leaching of the active metal oxides into the biodiesel mixture leading to a reduction in active sites (see figure 9) [56].

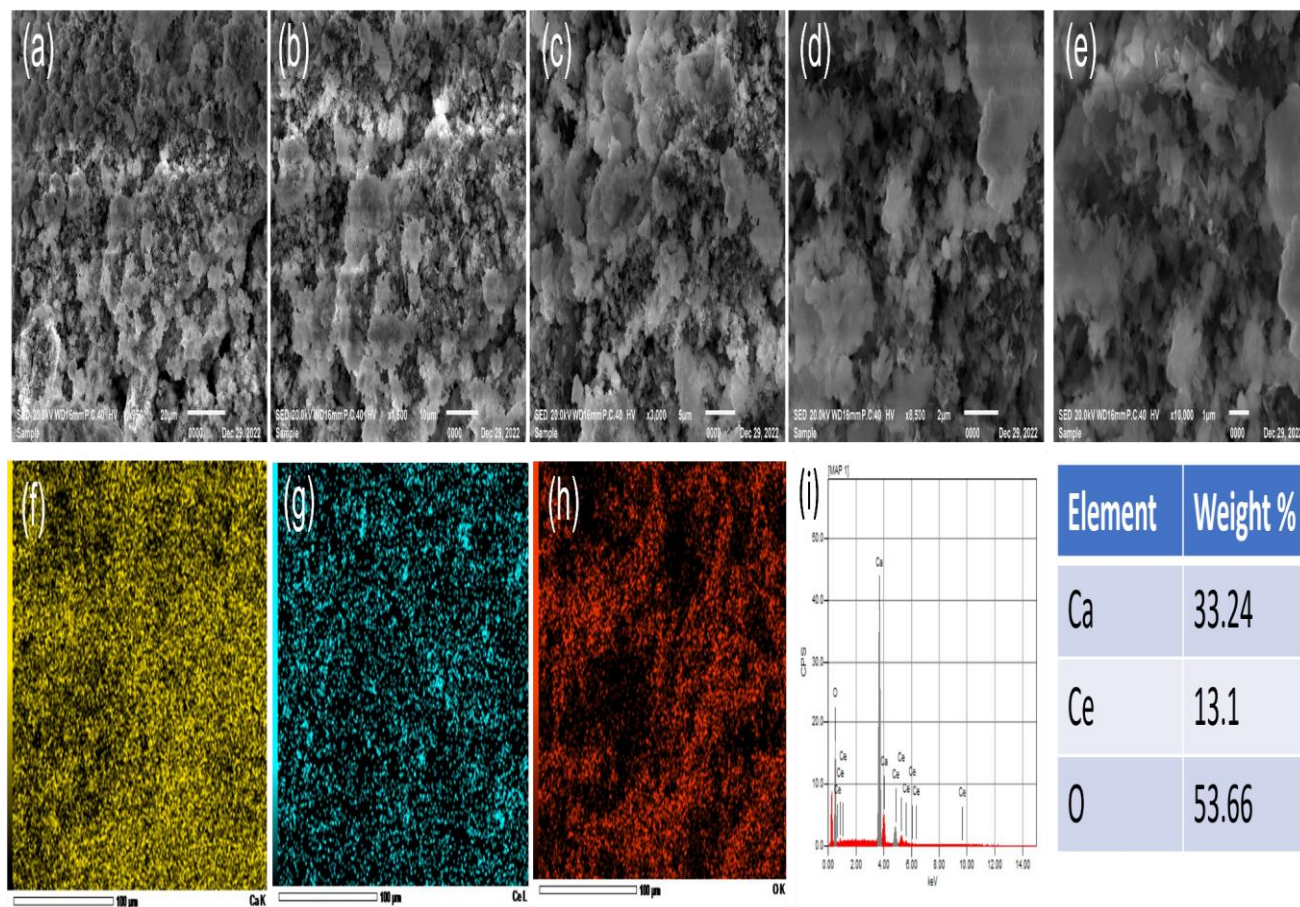


Figure 4: (a-e) SEM images of 3CaO-1CeO₂ at different magnifications, (f-h) Mapping EDX overlay of Ca, Ce, O respectively, (i-j) EDX of 3CaO-1CeO₂.

Table 4: Basicity measurements and The Fame yield of binary oxide xCaO-yCeO₂ calcinated at 500 °C and 800 °C.

Name of sample	Basicity (mmol/g)	FAME yield (%)
CaO-500 °C	109	97
CaO-800 °C	95	97
CeO ₂ -500 °C	48	3
CeO ₂ -800 °C	50	1
1CaO-3CeO ₂ -500 °C	48	7
2CaO- 2CeO ₂ -500 °C	53	15
3CaO -1CeO ₂ -500 °C	56	29
1CaO-3CeO ₂ -800 °C	65	93
2CaO-2CeO ₂ -800 °C	68	94
3CaO-1CeO ₂ -800 °C	72	94

Table 5: Basicity measurements and the fame yield of binary oxide $x\text{CaO}-y\text{CuO}$ calcinated at 500 °C and 800 °C.

Name of sample	Basicity (mmol/g)	FAME yield (%)
CaO-500 °C	109	97
CaO-800 °C	95	97
CuO-500 °C	48	2
CuO-800 °C	37	4
1CaO-3CuO-500 °C	50	1
2CaO-2CuO-500 °C	53	4
3CaO-1CuO-500 °C	55	4
1CaO-3CuO-800 °C	60	85
2CaO-2CuO-800 °C	61	92
3CaO-1CuO-800 °C	62	93

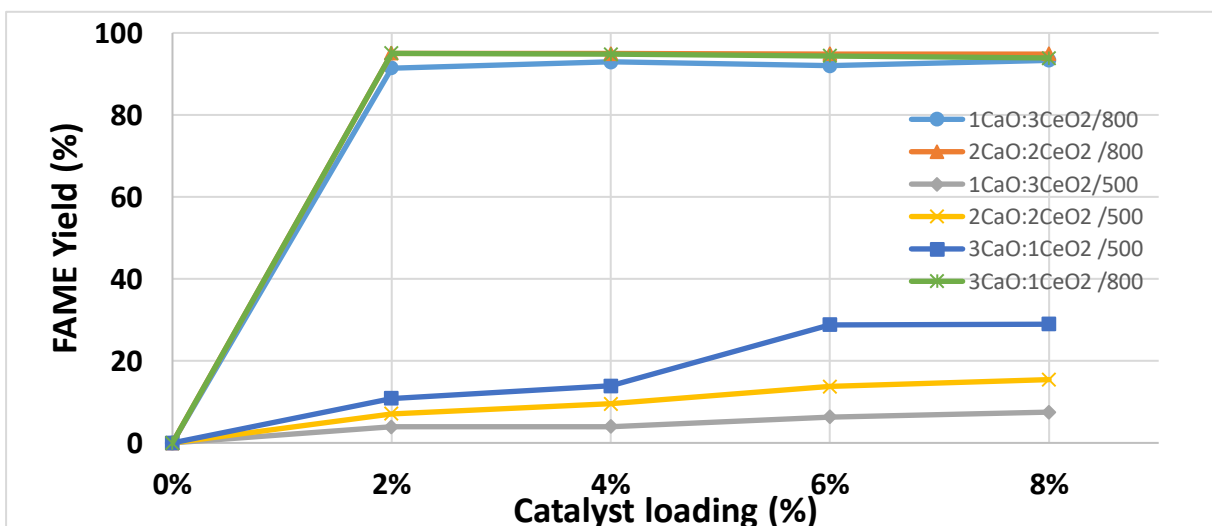
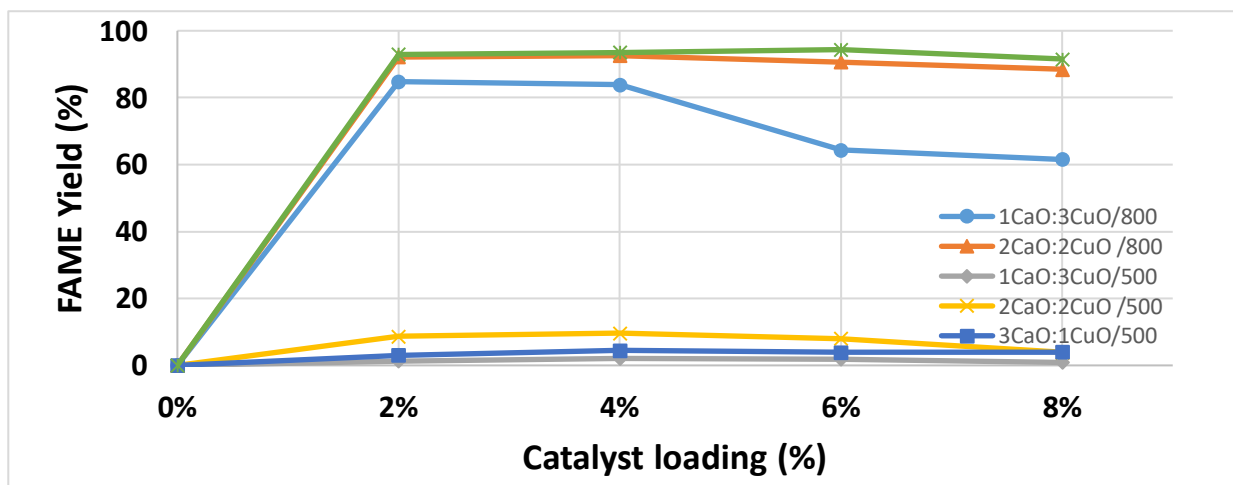

Fig. 5: The effect of catalyst loading $x\text{CaO}-y\text{CeO}_2$ -500/800 °C on the FAME yield %.

Fig. 6: The effect of catalyst loading $x\text{CaO}-y\text{CuO}$ -500/800 oC on the FAME yield %.

Table 6: Physicochemical properties of the obtained biodiesel using 3CaO-1CeO₂-800 °C in comparison with international biodiesel standards.

property	Unit	ASTM D-6751	Test method	Results	Reference
Density @15.5oC	kg m ⁻³	860–900	ASTM D-4052	900	[60]
Kinematic viscosity @40°C	mm ² s ⁻¹	1.9–6	ASTM D-445	6	[61]
Flash point	°C	Min. 130	ASTM D-93	168	[62]
Pour point	°C	–	ASTM D-97	6	[63]
Cloud point	°C	–	ASTM D-2500	12	[64]
Refractive index	–	–	ASTM D-1218	1.45461	[65]
Cetane index	–	–	ASTM D-976	32.5	[66]
Copper strip corrosion @100°C 3h	–	No.3	ASTM D-130	1b	[67]

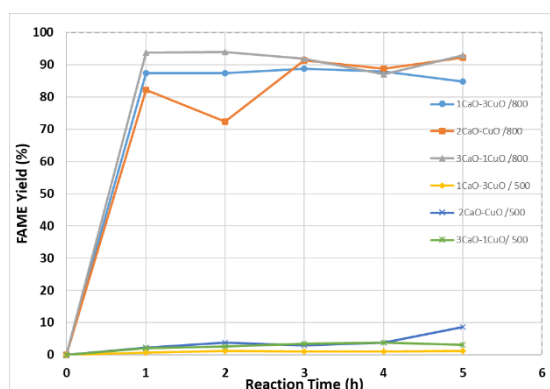


Fig.7: The effect of reaction time on the FAME yield of xCa-yCeO₂ @ 500/800°C.

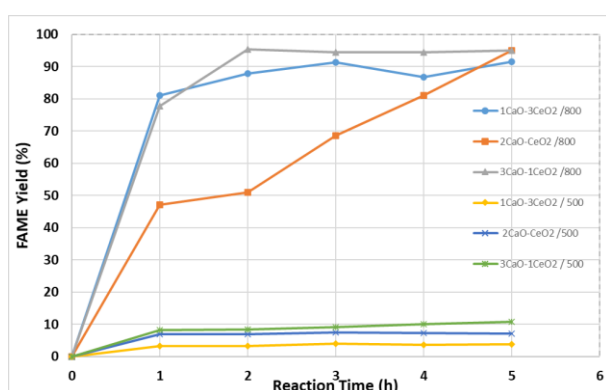


Fig. 8: The effect of reaction time on the FAME yield of xCa-yCuO @ 500/800 °C.

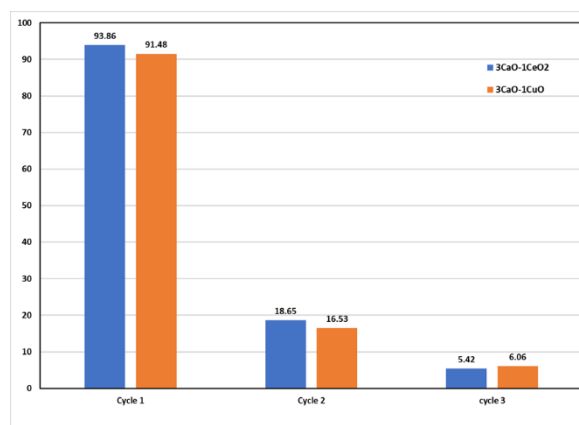


Fig. 9: The reusability test of (blue bar) 3CaO - 1CeO₂ and (orange bar) 3CaO - 1CuO catalyst for transesterification of WCO at optimum reaction conditions: catalyst loading = 2%, temperature = 75 °C, and M:O ratio = 13:1 for 5h and stirring rate = 300 rpm.

4. Fuel properties:

The properties of the produced biodiesel fuel at the optimum variable conditions (using 3CaO-1CeO₂-800 °C: catalyst loading level of 8%, reaction temperature of 75 °C, methanol /WCO molar ratio of 13:1 and reaction time of 5 h) are estimated according to international standards i.e., American

Standards for testing materials (ASTM) methods (e.g., density at 15.56 °C, kinematic viscosity at 40 °C, flash point, cloud point, pour point, refractive index, cetane index, and copper strip corrosion) (see Table 6). That is, the obtained results are comparable with the American (ASTM6751) biodiesel standards. It is noticed that the generated FAME has fitting values compared to the international standard value. That is, it can be used by biodiesel distributors for fueling diesel engines without any mechanical adjustment.

5. Conclusions

In this study, novel CaO–CeO₂ and CaO–CuO mixed oxide catalysts were successfully employed for the boosted transesterification of WCO into biodiesel. The as-synthesized catalysts were characterized by several techniques involving TGA, XRD, FT–IR, SEM–EDX, BET, and basicity measurement techniques to address the physicochemical criterion of the as-synthesized catalysts. Optimization of various operating parameters was conducted such as the w/w ratio of Ca concerning Ce and Cu, calcination temperature, catalyst loading level, and process duration. An optimum calcination temperature of 800 °C and catalyst loading of 2% for 2h was deduced as the optimum reaction conditions for the 3CaO:1CeO₂ while the optimum thermal treatment temperature of 800 °C for the 3CaO:1CuO and catalyst loading of 2% for 1 h was chosen as the optimum process conditions for attaining FAME yield of 94 and 93%, respectively. In summary, it was clarified that the addition of basic CaO oxides to the acidic (e.g., CeO₂ and CuO) resulted in an improvement of their catalytic performance towards the transesterification of waste cooking oil that is embodied in the high-rate FAME conversion rendering them as a tolerable catalyst for commercial biodiesel production. The produced FAME biofuel from waste oil via catalytic transesterification process unveiled beneficial combustibility criteria that are fulfill with American international standards (ASTM D-6751) under distinct climatic and environmental conditions.

Conflicts of interest

The authors declare that there are no conflicts of interest to declare.

References

- [1] Burke MJ, Stephens JC. Political power and renewable energy futures: A critical review. *Energy Res Soc Sci* 2018;35:78–93. <https://doi.org/10.1016/J.ERSS.2017.10.018>.
- [2] Sen S, Ganguly S. Opportunities, barriers and issues with renewable energy development – A discussion. *Renewable and Sustainable Energy Reviews* 2017;69:1170–81. <https://doi.org/10.1016/J.RSER.2016.09.137>.
- [3] Juan JC, Kartika DA, Wu TY, Hin TYY. Biodiesel production from jatropha oil by catalytic and non-catalytic approaches: An overview. *Bioresour Technol* 2011;102:452–60. <https://doi.org/10.1016/J.BIORTECH.2010.09.093>.
- [4] Mutezo G, Mulopo J. A review of Africa's transition from fossil fuels to renewable energy using circular economy principles. *Renewable and Sustainable Energy Reviews* 2021;137:110609. <https://doi.org/10.1016/J.RSER.2020.110609>.
- [5] Bozbas K. Biodiesel as an alternative motor fuel: Production and policies in the European Union. *Renewable and Sustainable Energy Reviews* 2008;12:542–52. <https://doi.org/10.1016/J.RSER.2005.06.001>.
- [6] Chia SR, Nomanbhay S, Ong MY, Shamsuddin AH Bin, Chew KW, Show PL. Renewable diesel as fossil fuel substitution in Malaysia: A review. *Fuel* 2022;314:123137.
- [7] Priya, Deora PS, Verma Y, Muhal RA, Goswami C, Singh T. Biofuels: An alternative to conventional fuel and energy source. *Mater Today Proc* 2022;48:1178–84. <https://doi.org/10.1016/J.MATPR.2021.08.227>.
- [8] Huang D, Zhou H, Lin L. Biodiesel: an Alternative to Conventional Fuel. *Energy Procedia* 2012;16:1874–85. <https://doi.org/10.1016/J.EGYPRO.2012.01.287>.
- [9] Rizk MR, Abd El-Moghny MG, Abdelhady HH, Ragheb WM, Mohamed AH, Fouad HF, et al. Tailor-designed bimetallic Co/Ni macroporous electrocatalyst for efficient glycerol oxidation and water electrolysis. *Int J Hydrogen Energy* 2022. <https://doi.org/10.1016/J.IJHYDENE.2022.07.129>.
- [10] Baibars IO, Abd El-Moghny MG, El-Deab MS. NiFeO_xH_y/Ni₃Fe interface design via electro passivation for superior catalysis of HER. *J Environ Chem Eng* 2022;10:108736. <https://doi.org/10.1016/J.JECE.2022.108736>.
- [11] Abdelrahim AM, El-Moghny MGA, El-Shakre ME, El-Deab MS. Tailor-designed Ni-Co binary hydroxide electrodes for boosted supercapacitor

- applications: Smart selection of additives. *Electrochim Acta* 2021;378:137991.
<https://doi.org/10.1016/J.ELECTACTA.2021.137991>.
- [12] Baibars IO, Abd El-Moghny MG, El-Deab MS. Boosted electrolytic hydrogen production at tailor-tuned nano-dendritic Ni-doped Co foam-like catalyst. *Electrochim Acta* 2022;410:139992.
<https://doi.org/10.1016/J.ELECTACTA.2022.139992>.
- [13] Abdelrahim AM, Abd El-Moghny MG, El-Shakre ME, El-Deab MS. Robust electrolytic oxygen evolution at nanostructured NiFe LDH@ in-situ functionalized graphite felt. *J Alloys Compd* 2023;967:171771.
<https://doi.org/10.1016/J.JALLCOM.2023.171771>.
- [14] Marulanda VF. Biodiesel production by supercritical methanol transesterification: process simulation and potential environmental impact assessment. *J Clean Prod* 2012;33:109–16.
<https://doi.org/10.1016/J.JCLEPRO.2012.04.022>.
- [15] Ma F, Hanna MA. Biodiesel production: a review. *BioresourTechnol* 1999;70:1–15.
[https://doi.org/10.1016/S0960-8524\(99\)00025-5](https://doi.org/10.1016/S0960-8524(99)00025-5).
- [16] Mawlid OA, Abdelhady HH, Abd El-Moghny MG, Hamada A, Abdelnaby F, Kased M, et al. Clean approach for catalytic biodiesel production from waste frying oil utilizing K₂CO₃/Orange peel derived hydrochar via RSM Optimization. *J Clean Prod* 2024;442:140947.
<https://doi.org/10.1016/J.JCLEPRO.2024.140947>.
- [17] Ibrahim MM, Elsaman HA, Hashish HMA, El-Sayed AB, Mostafa E. Effect of the Duration Time of Cooking Frequency on Chemical and Physical Properties of Waste Cooking Oil Used for Biodiesel Production. *Egypt J Chem* 2022;65:415–26.
<https://doi.org/10.21608/EJCHEM.2022.95410.5473>.
- [18] Kolo L, Soekamto NH, Firdaus, Taba P. Synthesis of MCM-48 contains NaCl and Surfactant as Catalyst in the Esterification of Nyamplung Oil (*Calophyllum inophyllum* L.) to Biodiesel. *Egypt J Chem* 2023;66:431–7.
<https://doi.org/10.21608/EJCHEM.2022.104616.4836>.
- [19] Khudhair MM, Mousa EF. Synthesis and characterization of biodiesel from seeds of castor plant. *Egypt J Chem* 2023;66:293–301.
<https://doi.org/10.21608/EJCHEM.2022.152391.6600>.
- [20] Abdelsadak Abdelwahab MY, Mustafa HMM, Gouda Z. A, Mokhtar MM, M AM, Ghareb MA, et al. The effect of temperature, time, and methanol concentration on enhancing the yield of biodiesel production of castor and rapeseed seeds via the Transesterification process. *Egypt J Chem* 2024;0:0–0.
- [21] Mohamed RM, Mustafa HMM, Shehata WM, Afify AA-M, Hassan GK, Shoab AM. Optimizing Operating Conditions for Maximum Biodiesel Production from Salmon Fish Oil. *Egypt J Chem* 2024;0:0–0.
<https://doi.org/10.21608/EJCHEM.2024.257532.9031>.
- [22] Knothe G, Razon LF. Biodiesel fuels. *Prog Energy Combust Sci* 2017;58:36–59.
<https://doi.org/10.1016/J.PECS.2016.08.001>.
- [23] Meher LC, Vidya Sagar D, Naik SN. Technical aspects of biodiesel production by transesterification—a review. *Renewable and Sustainable Energy Reviews* 2006;10:248–68.
<https://doi.org/10.1016/J.RSER.2004.09.002>.
- [24] Pinzi S, Garcia IL, Lopez-Gimenez FJ, DeCastro MDL, Dorado G, Dorado MP. The Ideal Vegetable Oil-based Biodiesel Composition: A Review of Social, Economical and Technical Implications. *Energy and Fuels* 2009;23:2325–41.
<https://doi.org/10.1021/EF801098A>.
- [25] Gardy J, Hassanpour A, Lai X, Ahmed MH, Rehan M. Biodiesel production from used cooking oil using a novel surface functionalised TiO₂ nanocatalyst. *Appl Catal B* 2017;207:297–310.
<https://doi.org/10.1016/J.APCATB.2017.01.080>.
- [26] Ahn BK, Wang H, Robinson S, Shrestha TB, Troyer DL, Bossmann SH, et al. Green Chemistry Ring opening of epoxidized methyl oleate using a novel acid-functionalized iron nanoparticle catalyst † 2012.
<https://doi.org/10.1039/c1gc16043e>.
- [27] Lam MK, Lee KT, Mohamed AR. Homogeneous, heterogeneous and enzymatic catalysis for transesterification of high free fatty acid oil (waste cooking oil) to biodiesel: A review. *Biotechnol Adv* 2010;28:500–18.
<https://doi.org/10.1016/J.BIOTECHADV.2010.03.002>.
- [28] Canakci M, Van Gerpen J. BIODIESEL PRODUCTION FROM OILS AND FATS WITH HIGH FREE FATTY ACIDS. *Transactions of the ASAE n.d.*;44:1429–36.
- [29] Demirbas A. Biodiesel from waste cooking oil via base-catalytic and supercritical methanol transesterification. *Energy Convers Manag* 2009;50:923–7.
<https://doi.org/10.1016/J.ENCONMAN.2008.12.023>.
- [30] Wen Z, Yu X, Tu ST, Yan J, Dahlquist E. Synthesis of biodiesel from vegetable oil with methanol catalyzed by Li-doped magnesium oxide catalysts. *Appl Energy* 2010;87:743–8.
<https://doi.org/10.1016/J.APENERGY.2009.09.013>.
- [31] Niju S, Raj FR, Anushya C, Balajii M. Optimization of acid catalyzed esterification and mixed metal oxide catalyzed transesterification for biodiesel production from *Moringa oleifera*

- oil. *Green Processing and Synthesis* 2019;8:756–75.
- [32] Habte L, Shiferaw N, Mulatu D, Thenepalli T, Chilakala R, Ahn JW. Synthesis of Nano-Calcium Oxide from Waste Eggshell by Sol-Gel Method. *Sustainability* 2019, Vol 11, Page 3196 2019;11:3196. <https://doi.org/10.3390/SU11113196>.
- [33] Yu X, Wen Z, Li H, Tu ST, Yan J. Transesterification of Pistacia chinensis oil for biodiesel catalyzed by CaO–CeO₂ mixed oxides. *Fuel* 2011;90:1868–74. <https://doi.org/10.1016/J.FUEL.2010.11.009>.
- [34] Abdelhady HH, Elazab HA, Ewais EM, Saber M, El-Deab MS. Efficient catalytic production of biodiesel using nano-sized sugar beet agro-industrial waste. *Fuel* 2020;261. <https://doi.org/10.1016/j.fuel.2019.116481>.
- [35] Saeed AMM, Sharma S, Hassan SZ, Ghaleb AM, Cao GP. Intensification and Optimization of FAME Synthesis via Acid-Catalyzed Esterification Using Central Composite Design (CCD). *ACS Omega* 2023;8:26206–17. https://doi.org/10.1021/ACSOMEGA.3C02434/ASSET/IMAGES/LARGE/AO3C02434_0018.JPG.
- [36] Kalita P, Basumatary B, Saikia P, Das B, Basumatary S. Biodiesel as renewable biofuel produced via enzyme-based catalyzed transesterification. *Energy Nexus* 2022;6:100087. <https://doi.org/10.1016/J.NEXUS.2022.100087>.
- [37] Miao X, Li R, Yao H. Effective acid-catalyzed transesterification for biodiesel production. *Energy Convers Manag* 2009;50:2680–4. <https://doi.org/10.1016/J.ENCONMAN.2009.06.021>.
- [38] Pathak S. Acid catalyzed transesterification. Available Online Www.Jocpr.Com *Journal of Chemical and Pharmaceutical Research* 2015;7:1780–6.
- [39] Cao Y, Dhahad HA, Esmaili H, Razavi M. MgO@CNT@K₂CO₃ as a superior catalyst for biodiesel production from waste edible oil using two-step transesterification process. *Process Safety and Environmental Protection* 2022;161:136–46. <https://doi.org/10.1016/J.PSEP.2022.03.026>.
- [40] Tamjidi S, KamyabMoghadas B, Esmaili H. Ultrasound-assisted biodiesel generation from waste edible oil using CoFe₂O₄@GO as a superior and reclaimable nanocatalyst: Optimization of two-step transesterification by RSM. *Fuel* 2022;327:125170. <https://doi.org/10.1016/J.FUEL.2022.125170>.
- [41] Mandari V, Devarai SK. Biodiesel Production Using Homogeneous, Heterogeneous, and Enzyme Catalysts via Transesterification and Esterification Reactions: a Critical Review. *BioEnergy Research* 2021 15:2 2021;15:935–61. <https://doi.org/10.1007/S12155-021-10333-W>.
- [42] Kalita P, Basumatary B, Saikia P, Das B, Basumatary S. Biodiesel as renewable biofuel produced via enzyme-based catalyzed transesterification. *Energy Nexus* 2022;6:100087. <https://doi.org/10.1016/J.NEXUS.2022.100087>.
- [43] Xie D, Ji X, Zhou Y, Dai J, He Y, Sun H, et al. Chlorella vulgaris cultivation in pilot-scale to treat real swine wastewater and mitigate carbon dioxide for sustainable biodiesel production by direct enzymatic transesterification. *BioresourTechnol* 2022;349:126886. <https://doi.org/10.1016/J.BIORTECH.2022.126886>.
- [44] Abu-Ghazala AH, Abdelhady HH, Mazhar AA, El-Deab MS. Valorization of hazard waste: Efficient utilization of white brick waste powder in the catalytic production of biodiesel from waste cooking oil via RSM optimization process. *Renew Energy* 2022;200:1120–33. <https://doi.org/10.1016/j.renene.2022.10.045>.
- [45] Abu-Ghazala AH, Abdelhady HH, Mazhar AA, El-Deab MS. Enhanced low-temperature production of biodiesel from waste cooking oil: aluminum industrial waste as a precursor of efficient CaO/Al₂O₃ nano-catalyst. *Fuel* 2023;351. <https://doi.org/10.1016/j.fuel.2023.128897>.
- [46] Mawlid OA, Abdelhady HH, El-Deab MS. Boosted biodiesel production from waste cooking oil using novel SrO/MgFe₂O₄ magnetic nanocatalyst at low temperature: Optimization process. *Energy Convers Manag* 2022;273:116435. <https://doi.org/10.1016/J.ENCONMAN.2022.116435>.
- [47] Mawlid OA, Abdelhady HH, El-Deab MS. Highly active novel K₂CO₃ supported on MgFe₂O₄ magnetic nanocatalyst for low-temperature conversion of waste cooking oil to biodiesel: RSM optimization, kinetic, and thermodynamic studies. *J Environ Chem Eng* 2023;11:110623. <https://doi.org/10.1016/J.JECE.2023.110623>.
- [48] Abu-Ghazala AH, Abdelhady HH, Mazhar AA, El-Deab MS. Exceptional room temperature catalytic transesterification of waste cooking oil to biodiesel using environmentally-benign K₂CO₃/γ-Al₂O₃ nano-catalyst. *Chemical Engineering Journal* 2023;474:145784. <https://doi.org/10.1016/J.CEJ.2023.145784>.
- [49] D6751 Standard Specification for Biodiesel Fuel Blend Stock (B100) for Middle Distillate Fuels n.d. <https://www.astm.org/d6751-20a.html> (accessed December 23, 2023).
- [50] Mofijur M, Masjuki HH, Kalam MA, Rasul MG, Atabani AE, Hazrat MA, et al. *ScienceDirect*

- Effect of Biodiesel-Diesel Blending on Physico-Chemical Properties of Biodiesel produced from *Moringa oleifera*. *Procedia Eng* 2015;105:665–9. <https://doi.org/10.1016/j.proeng.2015.05.046>.
- [51] Zhang N, Xue H, Hu R. The activity and stability of CeO₂@CaO catalysts for the production of biodiesel. *RSC Adv* 2018;8:32922–9. <https://doi.org/10.1039/C8RA06884D>.
- [52] Akhtar MT, Ahmad M, Shaheen A, Zafar M, Ullah R, Asma M, et al. Comparative study of liquid biodiesel from *Sterculia foetida* (bottle tree) using CuO-CeO₂ and Fe₂O₃ nano catalysts. *Front Energy Res* 2019;7:433358. <https://doi.org/10.3389/FENRG.2019.00004/BIBTEX>.
- [53] Phiwdang K, Suphankij S, Mekprasart W, Pecharapa W. Synthesis of CuO Nanoparticles by Precipitation Method Using Different Precursors. *Energy Procedia* 2013;34:740–5. <https://doi.org/10.1016/J.EGYPRO.2013.06.808>.
- [54] Hu C, Zhu Q, Jiang Z, Zhang Y, Wang Y. Preparation and formation mechanism of mesoporous CuO-CeO₂ mixed oxides with excellent catalytic performance for removal of VOCs. *Microporous and Mesoporous Materials* 2008;113:427–34. <https://doi.org/10.1016/J.MICROMESO.2007.11.043>.
- [55] Satapathy A, Saikia K, Rokhum SL. Biodiesel Production Using a Banana Peel Extract-Mediated Highly Basic Heterogeneous Nanocatalyst. *Sustainability (Switzerland)* 2023;15:11332.
- [56] Yu X, Wen Z, Li H, Tu ST, Yan J. Transesterification of *Pistacia chinensis* oil for biodiesel catalyzed by CaO-CeO₂ mixed oxides. *Fuel* 2011;90:1868–74. <https://doi.org/10.1016/J.FUEL.2010.11.009>.
- [57] Sivasamy A, Cheah KY, Fornasiero P, Kemausor F, Zinoviev S, Miertus S. Catalytic Applications in the Production of Biodiesel from Vegetable Oils. *ChemSusChem* 2009;2:278–300. <https://doi.org/10.1002/CSSC.200800253>.
- [58] Kesić Ž, Lukić I, Brkić D, Rogan J, Zdujić M, Liu H, et al. Mechanochemical preparation and characterization of CaO·ZnO used as catalyst for biodiesel synthesis. *Appl Catal A Gen* 2012;427–428:58–65. <https://doi.org/10.1016/J.APCATA.2012.03.032>.
- [59] Akhtar MT, Ahmad M, Shaheen A, Zafar M, Ullah R, Asma M, et al. Comparative study of liquid biodiesel from *Sterculia foetida* (bottle tree) using CuO-CeO₂ and Fe₂O₃ nano catalysts. *Front Energy Res* 2019;7:433358. <https://doi.org/10.3389/FENRG.2019.00004/BIBTEX>.
- [60] D4052 Standard Test Method for Density, Relative Density, and API Gravity of Liquids by Digital Density Meter. <https://www.astm.org/d4052-22.html> (accessed December 23, 2023).
- [61] D445 Standard Test Method for Kinematic Viscosity of Transparent and Opaque Liquids (and Calculation of Dynamic Viscosity). <https://www.astm.org/standards/d445> (accessed December 23, 2023).
- [62] D93 Standard Test Methods for Flash Point by Pensky-Martens Closed Cup Tester. <https://www.astm.org/d0093-20.html> (accessed December 23, 2023).
- [63] D97 Standard Test Method for Pour Point of Petroleum Products. <https://www.astm.org/d0097-17br22.html> (accessed December 23, 2023).
- [64] D2500 Standard Test Method for Cloud Point of Petroleum Products and Liquid Fuels. <https://www.astm.org/d2500-17a.html> (accessed December 23, 2023).
- [65] D1218 Standard Test Method for Refractive Index and Refractive Dispersion of Hydrocarbon Liquids. <https://www.astm.org/d1218-21.html> (accessed December 23, 2023).
- [66] D976 Standard Test Method for Calculated Cetane Index of Distillate Fuels. <https://www.astm.org/standards/d976> (accessed December 23, 2023).
- [67] D130 Standard Test Method for Corrosiveness to Copper from Petroleum Products by Copper Strip Test. <https://www.astm.org/standards/d130> (accessed December 23, 2023).